
Relational Reasoning On Graphs Using Opinion Dynamics

Yulong Yang* Bowen Feng* Keqin Wang
Naomi Leonard Adji Bousso Dieng Christine Allen-Blanchette
Princeton University, Princeton, USA
{yulong.yang, bf2192, keqin.wang}@princeton.edu
{naomi, adji, ca15}@princeton.edu

Abstract

From pedestrians to Kuramoto oscillators, interactions between agents govern how a multitude of dynamical systems evolve in space and time. Discovering how these agents relate to each other can improve our understanding of the often complex dynamics that underlie these systems. Recent works learn to categorize relationships between agents based on observations of their physical behavior. These approaches are limited in that the relationship categories are modelled as independent and mutually exclusive, when in real world systems categories are often interacting. In this work, we introduce a level of abstraction between the physical behavior of agents and the categories that define their behavior. To do this, we learn a mapping from the agents' states to their affinities for each category in a graph neural network. We integrate the physical proximity of agents and their affinities in a nonlinear opinion dynamics model which provides a mechanism to identify mutually exclusive categories, predict an agent's evolution in time, and control an agent's behavior. We demonstrate the utility of our model for learning interpretable categories for mechanical systems, and demonstrate its efficacy on several long-horizon trajectory prediction benchmarks where we consistently outperform existing methods.

1 Introduction

Multi-agent systems can be found in domains as diverse as astronomy [1, 2], biology [3, 4, 5], physics [6, 7], and sports [8, 9]. Understanding how these systems evolve in time can provide insights useful for the discovery of unknown physics, and the rules governing collective behavior. Predicting the evolution of complex systems is a fundamental challenge in the learning literature: early black-box models determine future states from past states without regard for contextual information [10, 11]; and more recent approaches improve upon these models by incorporating information such as environmental conditions and the behavior of other agents [12, 13, 14, 15, 16]. While incorporating contextual information has led to more powerful trajectory prediction models, the opacity of these models limits our ability to leverage them to better understand the role of inter-agent relationships in system evolution.

Recent work in relational reasoning attempts to address this limitation by explicitly modelling inter-agent relationships [17, 18, 19, 20, 21, 22]. Discovering inter-agent relationships is challenging since, in general, there are no ground truth labels, and the relevant relationships may be unknown at design time. Graph neural network (GNN) [23] based approaches such as [19, 20, 21, 22] encode inter-agent relationships in mutually exclusive categories. In [19] inter-agent relationships are modelled as time

*Equal contribution

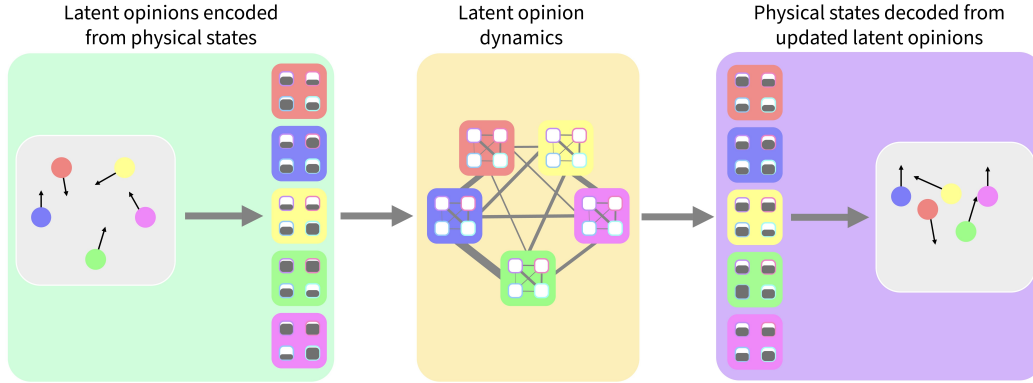


Figure 1: High level overview of RROD. RROD allows for relational reasoning by inter-agent relationships and inter-category interactions. The physical states of agents are encoded to latent affinities. Affinities are propagated forwards in time on the latent space in a nonlinear opinion dynamics model. The updated latent affinities are decoded into physical states as next step predictions.

invariant and optimized over entire trajectories. To improve expressivity, the authors of [20], model inter-agent relationships as time varying, and the authors of [21] represent the data in a hypergraph structure. While these methods improve multi-agent reasoning, the underlying assumption that inter-agent relationship categories are mutually exclusive diverges from what we observe in real world systems.

In the control and dynamics literature, practitioners model the evolution of agent affinities for predetermined categories using opinion dynamics. A recently popularized model, nonlinear opinion dynamics [24], has been used to model societal systems which respond quickly and flexibly to changes in environmental inputs [25, 26, 27, 28, 29, 30, 31, 32]. A limitation of this method, however, is that the relationship between an agent’s affinity for a category and it’s physical location must be known.

In our model, Relational Reasoning on graphs using Opinion Dynamics (RROD), we combine the flexibility of GNNs with the interpretability of nonlinear opinion dynamics for a new approach to relational reasoning. Concretely, our contributions are the following:

- In contrast to existing relational reasoning approaches which assume mutually exclusive relationship categories in the physical space, our model uses flexible and interacting relationship categories in a learned latent space.
- In contrast to existing opinion dynamics methods which require a known mapping between the space of agent’s physical locations and the space of their affinities, our model learns this mapping in a message passing neural network (MPNN) [33].
- Our model learns an interpretable latent space with a mechanism to identify mutually exclusive categories, predict an agent’s evolution in time, and control an agent’s behavior.

We demonstrate the utility of our approach for identifying mutually exclusive categories on multiple illustrative examples, and demonstrate the efficacy of our approach for trajectory prediction on both simulated and real world benchmarks.

2 Related Work

Trajectory prediction. In contrast to traditional control approaches which learn a set of model parameters from all available trajectories (i.e., sequences of physical positions) [34, 35, 36]; early approaches in deep learning learn to directly map an input sequence to future sequence states [11]. Later efforts incorporate external influences (e.g., behavior of other agents, environmental conditions) [12, 13, 14, 15, 16] and temporal dependencies [16, 37, 38, 39, 40]; and recent work uses graph based methods to model multi-agent dynamics [41, 42]. While these perform well on future

prediction tasks, they do not predict which agents interact or how they interact, a limitation which motivates relational reasoning.

Relational reasoning. The goal of relational reasoning is to infer inter-agent relationships in a multi-agent system [17, 19, 20, 21, 22]. In general, this task is challenging since the relationships between agents is unknown. Approaches to this challenge include: CommNet [17] which learns a continuous communication protocol for fully cooperative multi-agent tasks; Neural Relational Inference [19] which learns a time invariant inter-agent relationships; Dynamic Neural Relational Inference [20] which learns time varying inter-agent relationships; GroupNet [21] which uses a multiscale hypergraph representation of the input for improved expressivity; and EquiMotion [22] which incorporates an equivariance constraint to ensure the dynamics transform predictably to Euclidean shifts of the input data. Our work differs from these approaches in our representation of relationship categories. Our categories exist in the space of agent affinities rather than the physical space, and our categories flexible and interacting, rather than mutually exclusive and independent.

Consensus dynamics. In control and robotics, consensus dynamics [43] have been used in a myriad of settings to model the dynamics and control the behavior of multi-agent systems. In [44], the authors propose a linear model for prediction and control of multi-agent systems. In [45], the authors use a linear consensus dynamics model for coordinated surveying with underwater gliders. In [46], the authors use the consensus dynamics framework to develop rectilinear and circular consensus control laws for multi-vehicles systems. In [47], the authors use consensus dynamics to improve data collection in a mobile sensor network. In [48], the authors use consensus dynamics understand the robustness of starling flocking behavior. Even with this breadth of application, there are several draw backs to a purely linear model of opinion formation; specifically, the resulting dynamics always yield consensus and the formation of opinions in response to inputs is slow.

Nonlinear opinion dynamics. The noted short comings of linear consensus dynamics models, are resolved in the nonlinear opinion dynamics model proposed in [24]. Because the model is nonlinear, the dynamics a bifurcation and opinions can evolve to dissensus quickly. Nonlinear opinion dynamics have been used to model a variety of systems. In [25, 26, 27, 28] nonlinear opinion dynamics model information spread in settings such as political polarisation. In [29], nonlinear opinion dynamics is used to resolve deadlock, and in [30], it’s used for collision avoidance. In [31, 32], nonlinear opinion dynamics is used for task switching in robotic swarms in trash collecting robot teams. In contrast to these works, where the model has direct access agent opinions (i.e., affinities), we learn a mapping between physical states and agent opinions (i.e., affinities).

3 Background

In this section we provide a brief overview of the nonlinear opinion dynamics model proposed in [49]. The nonlinear nature of the model gives rise to bifurcations [50, 51] which provide a level of flexibility not possible with linear models. We use a restricted form of this model in our approach, which retains sufficient flexibility for our applications. We use the language of opinions and affinities interchangeably.

3.1 Nonlinear opinion dynamics

We define a multi-agent system as a system of $\mathcal{N}_a \in \mathbb{N}$ agents, each with a real-valued opinion on $\mathcal{N}_o \in \mathbb{N}$ categories. An agent’s opinion can be positive, negative or neutral, and the strength of its opinion is corresponds to the magnitude of its opinion. The change in an agent’s opinion on a particular category is determined by a combination of intrinsic and extrinsic parameters. Specifically, the change in agent i ’s opinion on category j is determined the nonlinear differential equation,

$$\dot{z}_{ij} = -d_{ij}z_{ij} + \mathcal{S} \left(u_i \left(\alpha_{ij}z_{ij} + \sum_{\substack{k=1 \\ k \neq i}}^{\mathcal{N}_a} a_{ik}^a z_{kj} + \sum_{\substack{l=1 \\ l \neq j}}^{\mathcal{N}_o} a_{jl}^o z_{il} + \sum_{\substack{k=1 \\ k \neq i}}^{\mathcal{N}_a} \sum_{\substack{l=1 \\ l \neq j}}^{\mathcal{N}_o} a_{ik}^a a_{jl}^o z_{kl} \right) \right) + b_{ij}, \quad (1)$$

where the parameters intrinsic to the agent $d_{ij} \geq 0$, $u_i \geq 0$, and $\alpha_{ij} \geq 0$, determine how resistant the agent is to forming an opinion, how attentive the agent is to the opinions of other agents, and

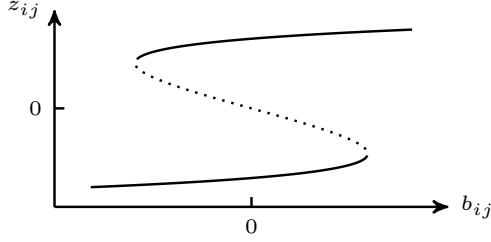


Figure 2: Opinion z_{ij} bifurcation diagram. The number and stability of equilibria changes with the agent dependent environmental input parameter b_{ij} . The solid line represents stable equilibria and dotted line represents unstable equilibria.

how resistant the agent is to changing its opinion; the parameters extrinsic to the agent b_{ij} , a_{jk}^a , and a_{jl}^o , determine the impact of the environment on the opinion the agent forms, its physical proximity to other agents and the interdependence of categories; and \mathcal{S} is a saturating function (e.g., \tanh) satisfying $\mathcal{S}(0) = 0$, $\mathcal{S}'(0) = 1$, and $\mathcal{S}'''(0) \neq 0$ [24].

For the remainder of this work, we use a vectorized form of equation (1),

$$\dot{\mathbf{z}} = -\mathbf{d} \odot \mathbf{z} + \mathcal{S} \left(\mathbf{u} \odot \left(\boldsymbol{\alpha} \odot \mathbf{z} + \mathbf{A}^a \mathbf{z} + \mathbf{z} \mathbf{A}^{o\top} + \mathbf{A}^a \mathbf{z} \mathbf{A}^{o\top} \right) \right) + \mathbf{b}, \quad (2)$$

where $\mathbf{A}^a = [a_{ik}^a]$ is the hollow inter-agent communication graph, and $\mathbf{A}^o = [a_{jl}^o]$ is the graph representing interdependence of categories.

Open-loop attention. We consider a restricted form of Equation (1) where the attention parameter u_i of each agent is fixed (i.e., the open-loop attention model [52, 24]). With this constraint, the resulting bifurcation diagram has the structure illustrated in Figure 2. Opinions can be steered to a desired sign and magnitude by varying the environmental input parameter b_{ij} . We leverage this capability in our approach for flexible and interpretable dynamics.

4 Method

In this section we present our model for relational reasoning. For a given multi-agent system, our goal is to infer both the relationships between agents, and how those relationships determine agent dynamics. We define a multi-agent system as a system of $\mathcal{N}_a \in \mathbb{N}$ agents, each with a real-valued affinities for $\mathcal{N}_o \in \mathbb{N}$ categories. We learn a mapping between the agents' states and their affinities for each category and how affinities evolve in time. The data used to train our model consists of N trajectories of T observations, where each observation has dimension d . For a specific trajectory, we denote the observation of agent i at time t , $\mathbf{x}_{i,t}$, and the affinities of agent i at time t , $\mathbf{z}_{i,t}$.

4.1 Encoders

We use separate encoding networks to learn mappings from agent states to agent affinities, and agent states to environmental inputs. We refer to the first of these encoders as the affinity encoder E_z , and the latter as the environmental input encoder E_b . Each encoder takes observations of the multi-agent system at time t as input and processes them in an MPNN [33]. The multi-agent system is represented as a fully-connected graph with node values determined by the physical state of each agent and edge weights determined by inter-agent proximity.

Formally, our affinity encoder E_z performs the following message passing functions for agent i at timestep t :

$$\mathbf{z}_{i,t}^1 = f_{\text{emb}}^z(\mathbf{x}_{i,t}), \quad (3)$$

$$v \rightarrow e: \quad \mathbf{m}_{(i,k),t}^z = f_e^z(\mathbf{z}_{i,t}, \mathbf{z}_{k,t}), \quad (4)$$

$$e \rightarrow v: \quad \mathbf{z}_{i,t}^2 = \mathbf{z}_{i,t}^1 + f_v^z \left(\sum_{k \neq i} \mathbf{m}_{(i,k),t}^z \right), \quad (5)$$

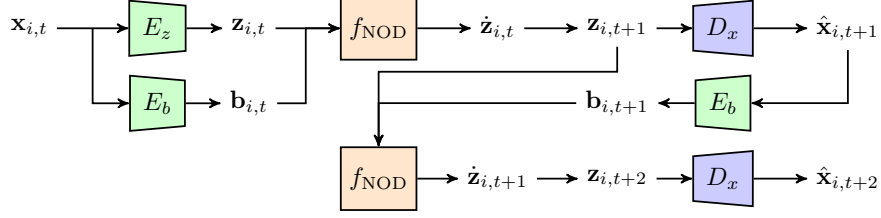


Figure 3: Overview of the RROD architecture. A graph neural network E_z encodes physical states into latent opinions. A graph neural network E_b encodes physical states into latent environmental inputs. The latent nonlinear opinion dynamics block f_{NOD} updates agents’ latent opinions. A graph neural network D_x decodes the updated latent opinions to updated physical states. The model’s latent dynamics are unrolled for trajectory prediction pass single-step.

where f_{emb}^z , f_e^z , and f_v^z are 3-layer MLPs. The environmental input encoder E_b is designed similarly, and performs the following message passing functions for agent i at timestep t :

$$\mathbf{b}_{i,t}^1 = f_{\text{emb}}^b(\mathbf{x}_{i,t}), \quad (6)$$

$$v \rightarrow e: \quad \mathbf{m}_{(i,k),t}^b = f_e^b(\mathbf{b}_{i,t}, \mathbf{b}_{k,t}), \quad (7)$$

$$e \rightarrow v: \quad \mathbf{b}_{i,t} = \mathbf{b}_{i,t}^2 = f_v^b\left(\sum_{k \neq i} \mathbf{m}_{(i,k),t}^b\right), \quad (8)$$

where f_{emb}^b , f_e^b , and f_v^b are 3-layer MLPs.

4.2 Latent nonlinear opinion dynamics

We use the nonlinear opinion dynamics formulation in equation (2) to model the evolution of agent affinities in the latent space,

$$\dot{\mathbf{z}}_t = f_{\text{NOD}}(\mathbf{z}_t, \mathbf{b}_t, \mathbf{A}_t^a) = -\mathbf{d} \odot \mathbf{z}_t + \mathcal{S}\left(\mathbf{u} \odot \left(\boldsymbol{\alpha} \odot \mathbf{z}_t + \mathbf{A}_t^a \mathbf{z}_t + \mathbf{z}_t \mathbf{A}_t^{a\top} + \mathbf{A}_t^a \mathbf{z}_t \mathbf{A}_t^{a\top}\right)\right) + \mathbf{b}_t. \quad (9)$$

We learn the intrinsic agent parameters, \mathbf{d} , \mathbf{u} , and $\boldsymbol{\alpha}$, as well as the extrinsic parameter \mathbf{A}^o , and compute the inter-agent communication graph \mathbf{A}_t^a at each timestep t . We compute future states using Euler integration,

$$\mathbf{z}_{t+1} = \mathbf{z}_t + f_{\text{NOD}}(\mathbf{z}_t, \mathbf{b}_t, \mathbf{A}_t^a) \Delta t, \quad (10)$$

where Δt is dataset dependent.

4.3 Decoder

We use a decoding network to learn a mapping from agent affinities to agent states. We refer to the decoder as D_x . Each decoder takes latent affinities of the multi-agent system at time t as input and processes them in an MPNN [33]. Latent affinities are represented as a fully-connected graph with node values determined by the affinities of each agent and edge weights determined by inter-agent proximity.

Formally, our decoder D_x performs the following message passing functions for agent i at timestep t :

$$\hat{\mathbf{x}}_{i,t}^1 = f_{\text{dec}}(\mathbf{z}_{i,t}), \quad (11)$$

$$v \rightarrow e: \quad \mathbf{m}_{(i,k),t}^x = f_e^x(\hat{\mathbf{x}}_{i,t}, \hat{\mathbf{x}}_{k,t}), \quad (12)$$

$$e \rightarrow v: \quad \hat{\mathbf{x}}_{i,t} = \hat{\mathbf{x}}_{i,t}^2 = f_v^x\left(\sum_{k \neq i} \mathbf{m}_{(i,k),t}^x\right), \quad (13)$$

where f_{emb}^x , f_e^x , and f_v^x are 3-layer MLPs

4.4 Loss function

We train our model using the three component loss function,

$$\mathcal{L} = \mathcal{L}_{\text{pred}} + \gamma_1 \mathcal{L}_{\text{recon}} + \gamma_2 \mathcal{L}_{\text{latent}} \quad (14)$$

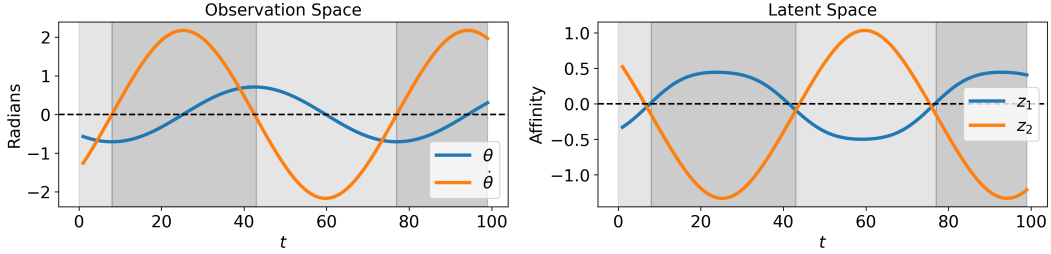


Figure 4: Learned affinity encodings on the pendulum dataset. The physical state of the pendulum bob (left). The learned representation of affinities (right). The affinities are perfectly out of phase indicating they are mutually exclusive.

where $\mathcal{L}_{\text{pred}}$ is the prediction loss, $\mathcal{L}_{\text{recon}}$ is the reconstruction loss and $\mathcal{L}_{\text{latent}}$ is the latent loss.

The prediction loss, $\mathcal{L}_{\text{pred}}$, is defined as the dissimilarity between the ground truth future state \mathbf{x}_t , and the predicted future state $\hat{\mathbf{x}}_t$, specifically,

$$\mathcal{L}_{\text{pred}} = \frac{1}{T} \sum_{t=1}^T \left\| \mathbf{x}_t - \hat{\mathbf{x}}_t \right\|^2, \quad (15)$$

and encourages accuracy of future state prediction. The reconstruction loss, $\mathcal{L}_{\text{recon}}$, is defined as the dissimilarity between the ground truth initial state \mathbf{x}_0 , and the reconstructed initial state $\hat{\mathbf{x}}_0$, specifically,

$$\mathcal{L}_{\text{recon}} = \left\| \mathbf{x}_0 - (D_x \circ E_z)(\mathbf{x}_0) \right\|^2, \quad (16)$$

and encourages the decoder to function as the inverse of the encoder. The latent loss, $\mathcal{L}_{\text{latent}}$, is defined as the dissimilarity of agent affinities predicted by the dynamical model, and those predicted by the affinity encoder, specifically,

$$\mathcal{L}_{\text{latent}} = \frac{1}{T} \sum_{t=1}^T \left\| \mathbf{z}_t - E_z(\mathbf{x}_t) \right\|^2, \quad (17)$$

and encourages alignment between the affinity dynamics module and encoder.

5 Experiments

In this section we present empirical results of our model on relational reasoning tasks. We demonstrate the utility of our approach for dimensionality reduction and trajectory prediction. We achieve dimensionality reduction by leveraging the ability of our model to identify mutually exclusive categories; and apply our model to trajectory prediction in the context of mechanical systems and pedestrian behavior. Data generation and training parameters are given in Appendix A and B respectively.

5.1 Interpretability of the latent space

Pendulum. We generate a synthetic dataset of pendulum motion where pendulum dynamics are defined by the second order equation,

$$\ddot{\theta} = -\frac{g}{\ell} \sin \theta, \quad (18)$$

with $\ell = 1.0$, $g = 9.81$, and initial conditions sampled from the uniform distribution, $\theta_0, \dot{\theta}_0 \sim \mathcal{U}(-0.5\pi, 0.5\pi)$. The dataset consists of 50000 training trajectories, and 12500 validation and testing trajectories.

The pendulum system is represented as a multi-agent system with a single agent i.e., the pendulum bob. We construct a graphical representation of this system where the node features are defined as the concatenation of the position and velocity of the pendulum bob, and there are no edges.

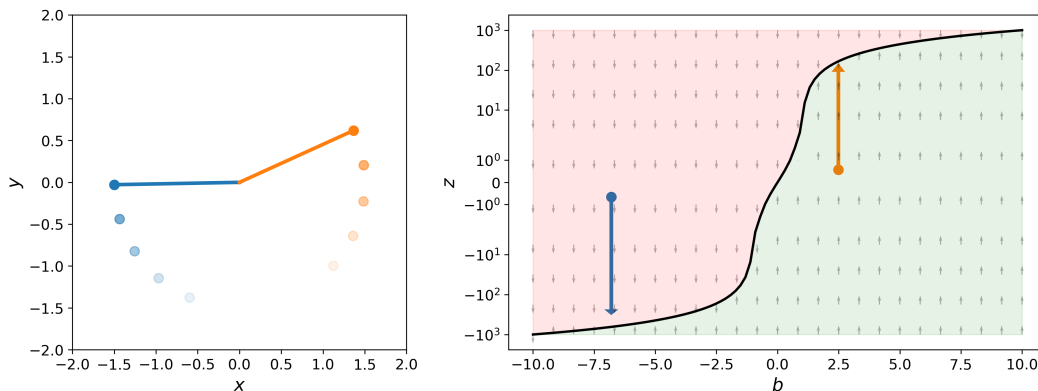


Figure 5: Learned affinity bifurcation diagram on the pendulum dataset. The physical behavior of the pendulum bob (left). The learned affinity bifurcation diagram (right). Clockwise motion (blue) and counterclockwise motion (orange) are mapped by the environmental input encoder to inputs that push the motion in opposite directions.

With this dataset, we demonstrate the interpretability of our latent categories and the ability of our model to identify mutually exclusive categories, a capability that can be used for dimensionality reduction (see Figure 4). The learned categories can be interpreted as clockwise motion and counterclockwise motion. We also illustrate how environmental input controls agent behavior (see Figure 5). When the pendulum bob is moving clockwise, the environmental input encoder produces a negative value for b , which changes the equilibrium value of the associated affinity z and causes it to change rapidly.

Double pendulum. We generate a synthetic dataset of double pendulum motion where double pendulum dynamics are defined by the second order equations in [53]. The pendulum arms are defined $\ell_1 = \ell_2 = 1.0$, pendulum bobs are defined $m_1 = m_2 = 1.0$, gravity is defined $g = 9.81$ and the initial conditions are sampled from the normal distribution, i.e., $\theta_{1,0}, \dot{\theta}_{1,0}, \theta_{2,0}, \dot{\theta}_{2,0} \sim \mathcal{N}(0, 0.5)$. The dataset consists of 50000 training trajectories, and 12500 validation and testing trajectories.

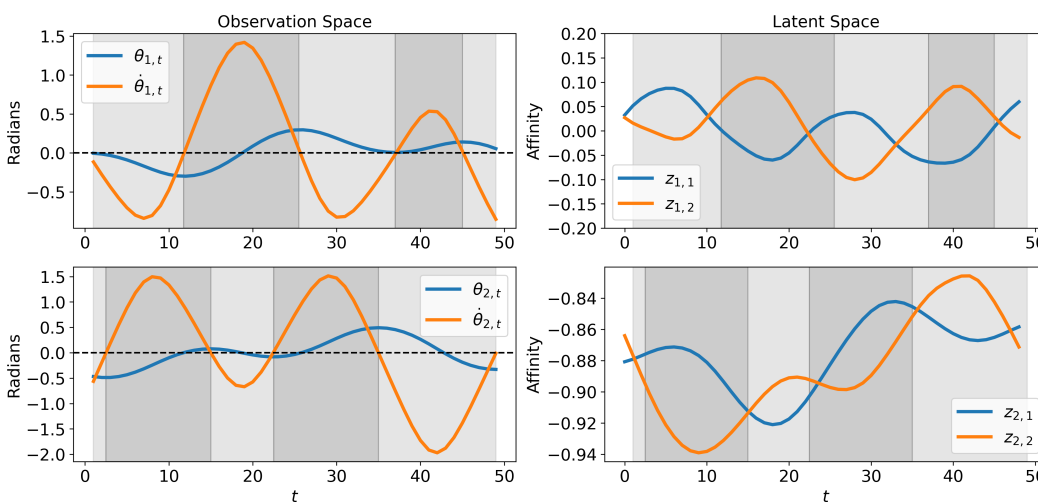


Figure 6: Latent affinities for the double pendulum. The physical state of the pendulum (left column). The learned representation of affinities (right column). The time when switching of the dominating affinity (higher valued) occurs corresponds to the time of switching between clockwise and counterclockwise (and vice versa) motion of the pendulums.

Table 1: Prediction MSE of test sets of Mass-Spring, Kuramoto, and TrajNet++ datasets. We train and compare RROD (ours, marked with *) with baseline models.

Network	Mass-Spring	Kuramoto	TrajNet++
RROD*	2.88×10^{-4}	4.52×10^{-3}	1.20×10^{-2}
NRI	3.73×10^{-3}	8.20×10^{-3}	8.49×10^{-2}
dNRI	4.86×10^{-3}	6.41×10^{-3}	4.00×10^{-2}

The double pendulum system is represented as a multi-agent system with two agents i.e., the pendulum bobs. We construct a graphical representation of this system where the node features are defined as the concatenation of the position and velocity of the pendulum bobs, and the edges correspond to connecting pendulum arms. Since the forces exerted by each bob on the other is equal in magnitude and opposite in direction, we construct the inter-agent communication matrix such that

$$\mathbf{A}_{(i,k),t}^a = (\mathbf{x}_{i,t} - \mathbf{x}_{k,t}). \quad (19)$$

With this dataset, we demonstrate interpretability of our latent categories in a more complicated setting. The learned categories can be interpreted as encoding when the pendulum switches from clockwise (positive) to counterclockwise (negative) (see 6). When this occurs, the affinity z_1 switches from the higher-valued affinity to the lower-valued affinity.

5.2 Trajectory prediction

We perform trajectory prediction in the context of mechanical systems and pedestrian behavior. We show the qualitative performance of our model in Figure 7, and compare the quantitative performance of our model to the performance of NRI [19] and dNRI [20] in Table 1.

5.2.1 Mechanical systems

Mass spring system. We generate a synthetic dataset of mass spring motion where the mass spring dynamics are defined by the second order equation,

$$\ddot{\mathbf{r}}_i = \sum_{i \neq j}^{N_a} -k_{ij} (\mathbf{r}_i - \mathbf{r}_j), \quad (20)$$

where the spring constant k_{ij} is randomly sampled to be either 2.5 or 0, and $k_{ij} = k_{ji}$. The initial conditions are sampled from the normal distribution, $\mathbf{r}_{i,0}, \dot{\mathbf{r}}_{i,0} \sim \mathcal{N}(0, 0.3)$. The dataset consists of 50000 training trajectories, and 12500 validation and testing trajectories.

The mass spring system is represented as a multi-agent system with 5 agents. We construct a graphical representation of this system where the node features are defined as the concatenation of the position and velocity of the masses, and the edges corresponds to the connecting springs. Considering the force exerted on either masses by the spring is equal and proportion to the distance between the two masses, we construct the inter-agent communication matrix such that

$$\mathbf{A}_{(i,k),t}^a = \|\mathbf{x}_{i,t} - \mathbf{x}_{k,t}\|^2. \quad (21)$$

At test time, we provide our model with the initial physical observation and perform 49-step prediction and compare it with the ground truth simulation. The predicted trajectories from the testing set is shown in Figure 7.

Kuramoto oscillator We generate a synthetic dataset of Kuramoto oscillator motion where the oscillator dynamics are defined by the first-order equation,

$$\dot{\phi}_i = \omega_i + \sum_{i \neq j} k_{ij} \sin(\phi_i - \phi_j), \quad (22)$$

where the coupling constant k_{ij} is randomly sampled to be either 2.5 or 0, and $k_{ij} = k_{ji}$. The initial conditions are sampled from the uniform distribution, $\phi_{i,t=0} \sim \mathcal{U}(0, 2\pi)$. The dataset consists of 50000 training trajectories, and 12500 validation and testing trajectories.

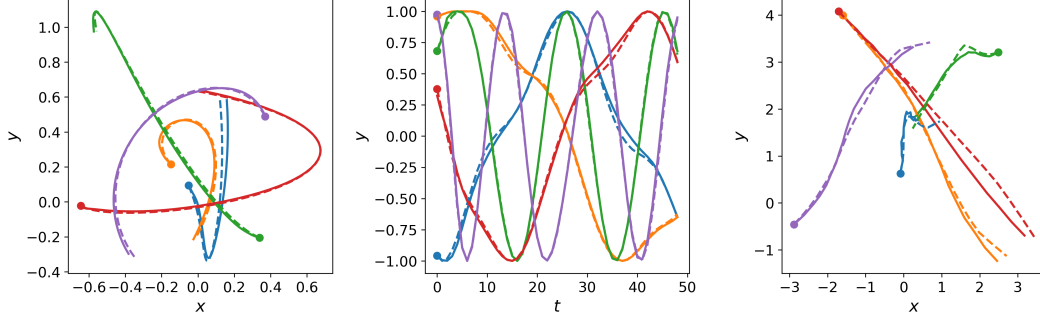


Figure 7: Comparison of the prediction (solid lines) and ground truth (dashed lines) trajectories generating using our model. From left to right are the mass spring, Kuramoto oscillator, and TrajNet++ dataset.

The Kuramoto oscillator is represented as a multi-agent system with 5 agents. We construct a graphical representation of this system where the node features are defined as the concatenation of the position and velocity of the Kuramoto oscillators, and the edges are connections between oscillators. Since \sin is an odd function, we construct the inter-agent communication matrix such that

$$\mathbf{A}_{(i,k),t}^a = (\mathbf{x}_{i,t} - \mathbf{x}_{k,t}). \quad (23)$$

At test time, we provide our model with the initial observation and perform 49-step prediction. We compute the MSE loss between our prediction and the ground truth. Predicted trajectories are shown in Figure 7.

5.2.2 Pedestrian behavior

TrajNet++. We evaluate our model on a synthetic subset of the TrajNet++ [54, 55] dataset where trajectories contain 5 agents. At test time, we provide our model with the initial observation and perform 19-step prediction. We compute the MSE loss between our prediction and the ground truth. The predicted trajectories from the testing set is shown in Figure 7.

We make the assumption that pedestrian sensing scales inversely with distance between agents, and construct the inter-agent communication matrix such that

$$\tilde{\mathbf{A}}_{(i,k),t}^a = \frac{c}{\|\mathbf{x}_{i,t} - \mathbf{x}_{k,t}\|^2 + \epsilon}, \quad (24)$$

where c and ϵ are constants. Since this is not a mechanical system, symmetric communication may not necessarily occur. We define the augmented communication matrix as

$$\mathbf{A}_{(i,k),t}^a = \mathbf{A}_{(i,k)}^{\text{pre}} \tilde{\mathbf{A}}_{(i,k),t}^a, \quad (25)$$

where $\mathbf{A}^{\text{pre}} \in \mathbb{R}^{\mathcal{N}_a \times \mathcal{N}_a}$ is a learnable pre-factor.

6 Conclusion

This paper proposes an alternative view of relational reasoning. Instead of focusing on interactions between physical states and using mutually exclusive relationship categories, we propose to model interactions between latent affinities of agents. Leveraging nonlinear opinion dynamics, our proposed method allows for more interpretability on the latent space. We can take advantage of this interpretability to understand how the latent space controls agent's physical behaviours. Lastly, we demonstrate that the proposed method outperforms existing methods.

Limitations and future work. Our pipeline generates sequences in a recurrent fashion, which can increase training time for long sequences [56]. Implementing teacher forcing [57] can reduce the required computational resources and time. Similarly to prior work, RROD assumes the same agents are present throughout a trajectory. Future work will investigate ways to use nonlinear opinion dynamics on graphs in an inductive manner.

References

- [1] Pablo Villanueva-Domingo, Francisco Villaescusa-Navarro, Daniel Anglés-Alcázar, Shy Genel, Federico Marinacci, David N Spergel, Lars Hernquist, Mark Vogelsberger, Romeel Dave, and Desika Narayanan. Inferring halo masses with graph neural networks. *The Astrophysical Journal*, 935(1):30, 2022.
- [2] Pablo Lemos, Niall Jeffrey, Miles Cranmer, Shirley Ho, and Peter Battaglia. Rediscovering orbital mechanics with machine learning. *Machine Learning: Science and Technology*, 4(4): 045002, 2023.
- [3] Edward Fiorelli, Naomi Ehrich Leonard, Pradeep Bhatta, Derek A Paley, Ralf Bachmayer, and David M Fratantoni. Multi-auv control and adaptive sampling in monterey bay. *IEEE journal of oceanic engineering*, 31(4):935–948, 2006.
- [4] George F Young, Luca Scardovi, Andrea Cavagna, Irene Giardina, and Naomi E Leonard. Starling flock networks manage uncertainty in consensus at low cost. *PLoS computational biology*, 9(1):e1002894, 2013.
- [5] Thomas D. Seeley, P. Kirk Visscher, Thomas Schlegel, Patrick M. Hogan, Nigel R. Franks, and James A. R. Marshall. Stop signals provide cross inhibition in collective decision-making by honeybee swarms. *Science*, 335(6064):108–111, 2012.
- [6] Emanuel Gull, Olivier Parcollet, and Andrew J Millis. Superconductivity and the pseudogap in the two-dimensional hubbard model. *Physical review letters*, 110(21):216405, 2013.
- [7] Antoine Browaeys and Thierry Lahaye. Many-body physics with individually controlled rydberg atoms. *Nature Physics*, 16(2):132–142, 2020.
- [8] Zhe Wang, Petar Veličković, Daniel Hennes, Nenad Tomašev, Laurel Prince, Michael Kaisers, Yoram Bachrach, Romuald Elie, Li Kevin Wenliang, Federico Piccinini, et al. Tacticalai: an ai assistant for football tactics. *Nature communications*, 15(1):1–13, 2024.
- [9] Sandro Hauri, Nemanja Djuric, Vladan Radosavljevic, and Slobodan Vucetic. Multi-modal trajectory prediction of nba players. In *Proceedings of the IEEE/CVF Winter Conference on Applications of Computer Vision*, pages 1640–1649, 2021.
- [10] Sepp Hochreiter and Jürgen Schmidhuber. Long short-term memory. *Neural computation*, 9(8): 1735–1780, 1997.
- [11] Ilya Sutskever, Oriol Vinyals, and Quoc V Le. Sequence to sequence learning with neural networks. *Advances in neural information processing systems*, 27, 2014.
- [12] Alexandre Alahi, Kratarth Goel, Vignesh Ramanathan, Alexandre Robicquet, Li Fei-Fei, and Silvio Savarese. Social lstm: Human trajectory prediction in crowded spaces. In *Proceedings of the IEEE conference on computer vision and pattern recognition*, pages 961–971, 2016.
- [13] Agrim Gupta, Justin Johnson, Li Fei-Fei, Silvio Savarese, and Alexandre Alahi. Social gan: Socially acceptable trajectories with generative adversarial networks. In *Proceedings of the IEEE conference on computer vision and pattern recognition*, pages 2255–2264, 2018.
- [14] Sergio Casas, Wenjie Luo, and Raquel Urtasun. Intentnet: Learning to predict intention from raw sensor data. In *Conference on Robot Learning*, pages 947–956. PMLR, 2018.
- [15] Nachiket Deo and Mohan M Trivedi. Convolutional social pooling for vehicle trajectory prediction. In *Proceedings of the IEEE conference on computer vision and pattern recognition workshops*, pages 1468–1476, 2018.
- [16] Amir Sadeghian, Vineet Kosaraju, Ali Sadeghian, Noriaki Hirose, Hamid Rezatofighi, and Silvio Savarese. Sophie: An attentive gan for predicting paths compliant to social and physical constraints. In *Proceedings of the IEEE/CVF conference on computer vision and pattern recognition*, pages 1349–1358, 2019.
- [17] Sainbayar Sukhbaatar, Rob Fergus, et al. Learning multiagent communication with backpropagation. *Advances in neural information processing systems*, 29, 2016.

- [18] Adam Santoro, David Raposo, David G Barrett, Mateusz Malinowski, Razvan Pascanu, Peter Battaglia, and Timothy Lillicrap. A simple neural network module for relational reasoning. *Advances in neural information processing systems*, 30, 2017.
- [19] Thomas Kipf, Ethan Fetaya, Kuan-Chieh Wang, Max Welling, and Richard Zemel. Neural relational inference for interacting systems. In *International conference on machine learning*, pages 2688–2697. PMLR, 2018.
- [20] Colin Graber and Alexander G Schwing. Dynamic neural relational inference. In *Proceedings of the IEEE/CVF Conference on Computer Vision and Pattern Recognition*, pages 8513–8522, 2020.
- [21] Chenxin Xu, Maosen Li, Zhenyang Ni, Ya Zhang, and Siheng Chen. Groupnet: Multiscale hypergraph neural networks for trajectory prediction with relational reasoning. In *Proceedings of the IEEE/CVF Conference on Computer Vision and Pattern Recognition*, pages 6498–6507, 2022.
- [22] Chenxin Xu, Robby T Tan, Yuhong Tan, Siheng Chen, Yu Guang Wang, Xinchao Wang, and Yanfeng Wang. Eqmotion: Equivariant multi-agent motion prediction with invariant interaction reasoning. In *Proceedings of the IEEE/CVF Conference on Computer Vision and Pattern Recognition*, pages 1410–1420, 2023.
- [23] Zonghan Wu, Shirui Pan, Fengwen Chen, Guodong Long, Chengqi Zhang, and S Yu Philip. A comprehensive survey on graph neural networks. *IEEE transactions on neural networks and learning systems*, 32(1):4–24, 2020.
- [24] Naomi Ehrich Leonard, Anastasia Bizyaeva, and Alessio Franci. Fast and flexible multiagent decision-making. *Annual Review of Control, Robotics, and Autonomous Systems*, 7, 2024.
- [25] Naomi Ehrich Leonard, Keena Lipsitz, Anastasia Bizyaeva, Alessio Franci, and Yphtach Lelkes. The nonlinear feedback dynamics of asymmetric political polarization. *Proceedings of the National Academy of Sciences*, 118(50):e2102149118, 2021.
- [26] Alessio Franci, Anastasia Bizyaeva, Shinkyu Park, and Naomi Ehrich Leonard. Analysis and control of agreement and disagreement opinion cascades. *Swarm Intelligence*, 15(1):47–82, 2021.
- [27] Wilbert Samuel Rossi and Paolo Frasca. Opinion dynamics with topological gossiping: Asynchronous updates under limited attention. *IEEE Control Systems Letters*, 4(3):566–571, 2020.
- [28] Abhimanyu Das, Sreenivas Gollapudi, and Kamesh Munagala. Modeling opinion dynamics in social networks. In *Proceedings of the 7th ACM international conference on Web search and data mining*, pages 403–412, 2014.
- [29] Haimin Hu, Kensuke Nakamura, Kai-Chieh Hsu, Naomi Ehrich Leonard, and Jaime Fernández Fisac. Emergent coordination through game-induced nonlinear opinion dynamics. In *2023 62nd IEEE Conference on Decision and Control (CDC)*, 2023.
- [30] Charlotte Cathcart, María Santos, Shinkyu Park, and Naomi Ehrich Leonard. Opinion-driven robot navigation: Human-robot corridor passing. 2022.
- [31] Anastasia Bizyaeva, Giovanna Amorim, María Santos, Alessio Franci, and Naomi Ehrich Leonard. Switching transformations for decentralized control of opinion patterns in signed networks: Application to dynamic task allocation. *IEEE Control Systems Letters*, 6:3463–3468, 2022.
- [32] Giovanna Amorim, María Santos, Shinkyu Park, Alessio Franci, and Naomi Ehrich Leonard. Threshold decision-making dynamics adaptive to physical constraints and changing environment. *arXiv preprint arXiv:2312.06395*, 2023.
- [33] Justin Gilmer, Samuel S Schoenholz, Patrick F Riley, Oriol Vinyals, and George E Dahl. Neural message passing for quantum chemistry. In *International conference on machine learning*, pages 1263–1272. PMLR, 2017.

- [34] Steven L Brunton, Joshua L Proctor, and J Nathan Kutz. Discovering governing equations from data by sparse identification of nonlinear dynamical systems. *Proceedings of the national academy of sciences*, 113(15):3932–3937, 2016.
- [35] Nicholas Galioto and Alex Arkady Gorodetsky. Bayesian system id: optimal management of parameter, model, and measurement uncertainty. *Nonlinear Dynamics*, 102(1):241–267, 2020.
- [36] Juan A Paredes, Yulong Yang, and Dennis S Bernstein. Output-only identification of self-excited systems using discrete-time lur’e models with application to a gas-turbine combustor. *International Journal of Control*, 97(2):187–212, 2024.
- [37] Karttikeya Mangalam, Harshayu Girase, Shreyas Agarwal, Kuan-Hui Lee, Ehsan Adeli, Jitendra Malik, and Adrien Gaidon. It is not the journey but the destination: Endpoint conditioned trajectory prediction. In *Computer Vision–ECCV 2020: 16th European Conference, Glasgow, UK, August 23–28, 2020, Proceedings, Part II 16*, 2020.
- [38] Anirudh Vemula, Katharina Muelling, and Jean Oh. Social attention: Modeling attention in human crowds. In *2018 IEEE international Conference on Robotics and Automation (ICRA)*, pages 4601–4607. IEEE, 2018.
- [39] Ye Yuan, Xinshuo Weng, Yanglan Ou, and Kris M Kitani. Agentformer: Agent-aware transformers for socio-temporal multi-agent forecasting. In *Proceedings of the IEEE/CVF International Conference on Computer Vision*, pages 9813–9823, 2021.
- [40] Francesco Giuliani, Irtiza Hasan, Marco Cristani, and Fabio Galasso. Transformer networks for trajectory forecasting. In *2020 25th international conference on pattern recognition (ICPR)*, pages 10335–10342. IEEE, 2021.
- [41] Cunjun Yu, Xiao Ma, Jiawei Ren, Haiyu Zhao, and Shuai Yi. Spatio-temporal graph transformer networks for pedestrian trajectory prediction. In *Computer Vision–ECCV 2020: 16th European Conference, Glasgow, UK, August 23–28, 2020, Proceedings, Part XII 16*, pages 507–523. Springer, 2020.
- [42] Jiyang Gao, Chen Sun, Hang Zhao, Yi Shen, Dragomir Anguelov, Congcong Li, and Cordelia Schmid. Vectornet: Encoding hd maps and agent dynamics from vectorized representation. In *Proceedings of the IEEE/CVF Conference on Computer Vision and Pattern Recognition*, pages 11525–11533, 2020.
- [43] Francesco Bullo. *Lectures on network systems*, volume 1. CreateSpace, 2018.
- [44] Herbert Levine, Wouter-Jan Rappel, and Inon Cohen. Self-organization in systems of self-propelled particles. *Physical Review E*, 63(1):017101, 2000.
- [45] Naomi E Leonard, Derek A Paley, Russ E Davis, David M Fratantoni, Francois Lekien, and Fumin Zhang. Coordinated control of an underwater glider fleet in an adaptive ocean sampling field experiment in monterey bay. *Journal of Field Robotics*, 27(6):718–740, 2010.
- [46] Eric W Justh and PS Krishnaprasad. Natural frames and interacting particles in three dimensions. In *Proceedings of the 44th IEEE Conference on Decision and Control*, pages 2841–2846. IEEE, 2005.
- [47] Naomi Ehrich Leonard, Derek A Paley, Francois Lekien, Rodolphe Sepulchre, David M Fratantoni, and Russ E Davis. Collective motion, sensor networks, and ocean sampling. *Proceedings of the IEEE*, 95(1):48–74, 2007.
- [48] Michele Ballerini, Nicola Cabibbo, Raphael Candelier, Andrea Cavagna, Evaristo Cisbani, Irene Giardina, Vivien Lecomte, Alberto Orlandi, Giorgio Parisi, Andrea Procaccini, et al. Interaction ruling animal collective behavior depends on topological rather than metric distance: Evidence from a field study. *Proceedings of the national academy of sciences*, 105(4):1232–1237, 2008.
- [49] Anastasia Bizyaeva, Alessio Franci, and Naomi Ehrich Leonard. Nonlinear opinion dynamics with tunable sensitivity. *IEEE Transactions on Automatic Control*, 68(3):1415–1430, 2022.

- [50] Martin Golubitsky, Ian Stewart, and David G Schaeffer. *Singularities and Groups in Bifurcation Theory: Volume II*, volume 69. Springer Science & Business Media, 2012.
- [51] Steven H Strogatz. *Nonlinear dynamics and chaos: with applications to physics, biology, chemistry, and engineering*. CRC press, 2018.
- [52] Anastasia Bizyaeva, Timothy Sorochkin, Alessio Franci, and Naomi Ehrich Leonard. Control of agreement and disagreement cascades with distributed inputs. In *2021 60th IEEE Conference on Decision and Control (CDC)*, pages 4994–4999. IEEE, 2021.
- [53] Double pendulum. <https://scienceworld.wolfram.com/physics/DoublePendulum.html>. Accessed: 2024-05-23.
- [54] Parth Kothari, Sven Kreiss, and Alexandre Alahi. Human trajectory forecasting in crowds: A deep learning perspective. *IEEE Transactions on Intelligent Transportation Systems*, 23(7): 7386–7400, 2021.
- [55] EPFL. Trajnet++ (a trajectory forecasting challenge), 2020. URL <https://www.aicrowd.com/challenges/trajnet-a-trajectory-forecasting-challenge>.
- [56] Antonio Orvieto, Samuel L Smith, Albert Gu, Anushan Fernando, Caglar Gulcehre, Razvan Pascanu, and Soham De. Resurrecting recurrent neural networks for long sequences. In *International Conference on Machine Learning*, pages 26670–26698. PMLR, 2023.
- [57] Ronald J Williams and David Zipser. A learning algorithm for continually running fully recurrent neural networks. *Neural computation*, 1(2):270–280, 1989.
- [58] Diederik P. Kingma and Jimmy Ba. Adam: A method for stochastic optimization. In *3rd International Conference on Learning Representations, ICLR*, 2015.

Appendix

A Datasets

In this section we provide data simulation and post processing steps for the dataset used in Section 5. Initial conditions are sampled according to distributions given in Section 5. Trajectories are simulated forward in time with a numerical integrator for a certain timestep and length, all given in Table 2. To reduce the dimensionality of the training data while preserving the dynamics of the system, the simulated trajectories are coarsened according to the frequency given in Table 2 to generate the final training data. We note that since Δt is passed into RROD as a fixed hyperparameter for training, the timestep of 1.0 is arbitrarily chosen for TrajNet++.

Table 2: Data generation and post processing parameters for experiments.

	Ideal Pendulum	Double Pendulum	Mass-Spring	Kuramoto	TrajNet++
Integrator	RK4	RK4	RK4	RK4	n/a
Δt	1e-3	5e-4	5e-4	5e-4	1.0
Steps	5000	5000	5000	500	n/a
Coarsening	100	100	100	10	n/a

B Training Details

In this section we provide training details on the experiments presented.

All models were trained on Dell Precision 7920 work stations. Each work station contains an Intel Xeon Gold 5220R 24 core CPU, two Nvidia A6000 GPUs, and 256GB of RAM. At training time only 1-GPU is used and the CPU and RAM is shared between two workloads. The hyperparameters used for training is given in Table 3.

Table 3: Hyperparameter for the experiments.

Hyperparameter	Ideal Pendulum	Double Pendulum	Mass-Spring	Kuramoto	TrajNet++
\mathcal{N}_a	1	2	5	5	5
\mathcal{N}_o	2	2	4	4	4
Epoch	500	500	1000	1000	1000
Batch Size	256	256	256	256	256
Activation	ReLU	ELU	tanh	tanh	tanh
Optimizer	Adam [58]	Adam	Adam	Adam	Adam
Learning Rate	1e-3	1e-3	1e-3	1e-3	5e-4
Hidden Dimension	64	64	128	128	128
Scheduler	N/A	N/A	StepLR	StepLR	StepLR
Scheduler Step	N/A	N/A	200	200	200
Scheduler Gamma	N/A	N/A	0.25	0.25	0.25
γ_1	1.0	1.0	1.0	1.0	1.0
γ_2	1.0	1.0	1.0	1.0	1.0